Natland, J.H., Dick H.J.B., Miller, D.J., and Von Herzen, R.P. (Eds.)
Proceedings of the Ocean Drilling Program, Scientific Results Volume 176

2. Data Report: Physical Properties Measurements in ODP Hole 735B[1]

R.A. Stephen[2]

INTRODUCTION

Hole 735B provides a unique opportunity to compare the in situ properties of a thick sequence of oceanic gabbros with the properties of oceanic Layer 3 observed seismically worldwide. For example, the correlation of laboratory tests, sonic log, and vertical seismic profile (VSP) compressional wave velocities from Hole 735B with typical refraction velocities of oceanic Layer 3 (6.5–6.8 km/s) was well established after the early work during Ocean Drilling Program (ODP) Leg 118 (Shipboard Scientific Party, 1989; Iturrino et al., 1991; Swift et al., 1991; Von Herzen et al., 1991). It was also observed, however, that there was anomalously high attenuation in the Site 735 gabbros (Goldberg et al., 1991, 1992; Swift and Stephen, 1992). If oceanic Layer 3 consisted largely of the types of gabbros observed at Site 735, then so much seismic energy would be absorbed on propagation through the crust that we would not observe mantle and Moho arrivals. Because we clearly do observe lower crustal and upper mantle arrivals on refraction seismic experiments, it was hypothesized that oceanic gabbros could compose only a small percentage of seismic Layer 3 material. A major objective of the physical properties program during Leg 176 was to test this hypothesis with measurements on additional cores from deeper in the section. Other objectives were to identify the nature of the reflections observed below the borehole during Leg 118 at depths of 560 and 760–825 meters below seafloor (mbsf) and to check for seismic anisotropy in the gabbros.

The "Physical Properties" section of the "Site 735" chapter in the Leg 176 *Initial Reports* volume (Shipboard Scientific Party, 1999) presents the results of shipboard measurements of compressional wave velocity. The average value of measurements on 217 minicores was 6.777 ± 0.292

[1]Stephen, R.A., 2001. Data report: Physical properties measurements in ODP Hole 735B. *In* Natland, J.H., Dick, H.J.B., Miller, D.J., and Von Herzen, R.P. (Eds.), *Proc. ODP, Sci. Results,* 176, 1–19 [Online]. Available from World Wide Web: <http://www-odp.tamu.edu/publications/176_SR/VOLUME/CHAPTERS/SR176_02.PDF>. [Cited YYYY-MM-DD]
[2]Woods Hole Oceanographic Institution, Woods Hole MA 02543, USA. **rstephen@whoi.edu**

Initial receipt: 7 April 2000
Acceptance: 24 July 2001
Web publication: 18 December 2001
Ms 176SR-017

km/s, which is in agreement with the Leg 118 results of 6.713 ± 0.383 km/s based on 228 minicores (Shipboard Scientific Party, 1989). These measurements were made at room temperature and pressure. We have carried out shore-based laboratory measurements on a small subset of the Leg 176 cores to (1) confirm the compressional wave velocities under in situ conditions of pressure, (2) measure shear wave velocities, (3) measure compressional and shear wave attenuation, and (4) check for anisotropy. For the last objective, we specifically acquired three sets of three mutually orthogonal whole-core samples.

METHODS

Table T1 summarizes the cores that were selected for shore-based analysis. Nine of the cores were sampled from the whole core and were 5–6 cm long. (Normal cores acquired from just the working half are typically 2–2.5 cm long.) Vertical cores (z) were cut through the center of the whole core before splitting. The cross-core sample (x) was acquired in the direction of splitting. The into-core sample (y) was acquired perpendicular to the direction of splitting. After splitting into the working and archival halves, looking down on the working half with up away from you, +z is to the top of the core, +x is to the right, and +y is down. The x and y cores are mutually perpendicular and subhorizontal, but they are not oriented azimuthally because the drill core is not oriented. All but two of the minicores were classified as olivine gabbros. The other two cores were a troctolitic gabbro and a gabbronorite. The cores were stored in seawater immediately after sampling and were kept saturated until the velocity and attenuation measurements were made. They were then dried to get the dry bulk density and saturation porosity information.

T1. Summary of cores analyzed, p. 18.

The density, porosity, and compressional and shear wave velocity data, as acquired by New England Research, Inc. (Coyner, 1984), are presented in "Appendix A," p. 7. The velocity measurements were made with the pulse-transmission technique. The confining pressure, P_c, was applied to the jacketed sample hydrostatically. The pore pressure, P_p, was kept at ~2 MPa. The velocities of compressional waves and of shear waves at two orthogonal polarizations through the core were made as confining pressure was increased from 10 to 200 MPa and then as pressure was decreased again. The difference in velocities at the same pressure measured during a pressure increase and during a pressure decrease is called hysteresis. Usually the velocities measured during the decrease are higher.

RESULTS

Density, Porosity, and Compressional and Shear Wave Velocity Data

It is commonly assumed that almost all of the microcracks in a core have closed at 200 MPa pressure. This is approximately the pressure that the rock would be under at depth in the lower crust. Ideally, the velocity increase with pressure should be greater for high-porosity samples because there are more voids to close. All of our samples had porosities <1%, but there was no correlation between porosity and the

velocity difference between 10 and 200 MPa or between porosity and velocity at 200 MPa (Fig. F1).

The compressional wave velocity at 200 MPa is shown as a function of density in Figure F2. Most of the velocities cluster between 6800 and 7000 m/s, but there are two anomalously high values (>7500 m/s) and one low value near 6660 m/s. The latter was measured in the gabbronorite. Also shown in Figure F2 are lines of constant mean atomic weight (Birch, 1961; Iturrino et al., 1991). All of our measurements fall between the lines for mean atomic weights (M) of 20 and 22 with most values near $M = 21$, which is predicted by Birch's law for common rocks.

The relationship between compressional and average shear wave velocity is shown in Figure F3 with lines of constant Poisson's ratio (σ). Half of our (12) samples have Poisson's ratios >0.30. This contrasts with the Leg 118 results from shallower depths in Hole 735B for which none of the (13) minicores measured had Poisson's ratios >0.3. Rocks with higher Poisson's ratios are less rigid. It is not clear why gabbros of essentially the same composition but from greater depth should be less rigid.

The mean compressional wave velocity of our Leg 176 cores at 200 MPa is 7007 ± 266 m/s compared to 7100 ± 200 m/s for the Leg 118 olivine gabbros. The mean density of our Leg 176 cores is 2.95 ± 0.11 g/cm³ compared to 2.95 ± 0.5 g/cm³ for the Leg 118 olivine gabbros. The mean shear wave velocity of our Leg 176 cores is 3780 ± 188 m/s compared to 3900 ± 100 m/s for the Leg 118 olivine gabbros. The mean V_p/V_s ratio of our Leg 176 cores is 1.855 ± 0.064 compared to 1.81 for the Leg 118 olivine gabbros. The mean Poisson's ratio of our Leg 176 cores is 0.294 ± 0.020 compared to 0.28 for the Leg 118 olivine gabbros. None of the Leg 176 cores measured in this study had porosities >1%, but in the Leg 118 study ~20% of the cores had porosities >1%. Clearly, the Leg 176 olivine gabbros acquired over depths from 450 to 1500 mbsf have very similar physical properties to the olivine gabbros from Leg 118 acquired at depths of <450 mbsf.

Compressional and Shear Wave Attenuation Data

Compressional and shear wave attenuations were measured in the same cores by New England Research, Inc., using the spectral ratio method (Toksöz et al., 1979). The results are summarized in "Appendix B," p. 11. The method compares the waveforms of a rock sample with attenuation and a reference sample, usually aluminum, with very little attenuation. It relies on the assumption that the received waveform will be modified slightly by the decrease in higher-frequency energy due to attenuation. If there is scattering caused by heterogeneities within the sample or there are multiple paths of arrivals from the sides of the sample, the waveforms will be dramatically altered and the method breaks down. Figures F4 and F5 summarize the steps in the method for a good waveform (P) and a bad waveform (S), respectively. The compressional wave attenuation values are reasonably good but the shear wave values may be questionable. This method was also used by Goldberg et al. (1991) to study compressional wave attenuation in the Leg 118 cores.

The quality factor, Q, has an inverse relationship to attenuation. Often attenuation is quoted as the quantity $1000/Q$. When $1000/Q$ is large, the attenuation is large. The mean compressional wave $1000/Q$ value for our Leg 176 cores at 200 MPa is 33.8 ± 21.2. This compares to a mean $1000/Q$ for the Leg 118 cores made at atmospheric pressure of 49.14 ± 32.03. Again there is little difference between cores from 450 to 1500 mbsf and cores from above 450 mbsf. The shear attenuation,

F1. Compressional wave velocity vs. porosity, p. 12.

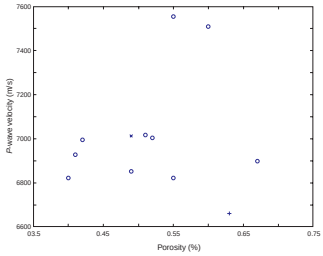

F2. Compressional wave velocity vs. saturated bulk density, p. 13.

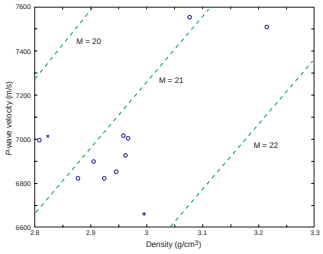

F3. Compressional wave velocity vs. shear wave velocity, p. 14.

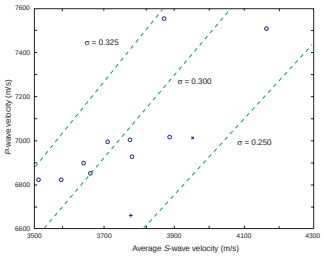

F4. Comparison of the spectra from an aluminum reference to the spectra for a gabbro sample, p. 15.

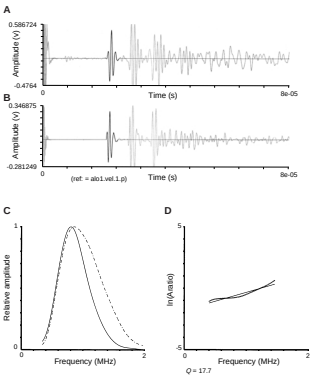

which was not measured on the Leg 118 cores, is 65.1 ± 30.9 for the Leg 176 cores. There is about twice as much shear wave attenuation as compressional wave attenuation.

Anisotropy

We investigated anisotropy by considering three sets of three orthogonal minicores selected from large macroscopically homogeneous sections of olivine gabbro. The directional velocity measurements are summarized in Table **T2.** The plus or minus "raw" or "measured" data from **"Appendix A,"** p. 7, have been "corrected" to a density datum of 2.95 g/cm^3 using Birch's Law, with a molecular weight of 21 (see below) and a V_p/V_s ratio of 1.85. Sections 176-735B-165R-5 and 193R-1 are essentially isotropic. Their compressional velocities are all within 117 m/s, compared to a standard deviation for *P*-wave velocities of 266 m/s. Similarly, their shear velocities are all within 147 m/s, compared to a standard deviation for *S*-wave velocities of 188 m/s.

For Section 176-735B-146R-2, however, there does appear to be significant variations in velocity with direction. After correction for density, the z-axis is dramatically slower for both compressional and shear waves. Anisotropy of the Leg 118 olivine gabbros was also discussed by Iturrino et al. (1991).

Empirical Relations for Oceanic Gabbros (V_p, V_s, and ρ)

It is often necessary in numerical modeling of seismic wave propagation in the oceanic crust to have simple empirical relationships between compressional wave velocity, shear wave velocity, and density. For example, a common relationship between compressional wave velocity (V_p, in kilometers per second) and density (ρ, in grams per cubic centimeter) for crustal rocks is as follows (from Ludwig et al., 1970):

$$\rho = 0.252 + 0.3788 \times V_p.$$

These are often arbitrary linearizations of complex phenomena. Based on the Leg 118 and 176 core measurements, we recommend the following guidelines. In the absence of other information, a good approximation for oceanic gabbros is to assume a Poisson's ratio of 0.30 to compute V_s from V_p and to use Birch's Law with a molecular weight of 21 at a pressure of 200 MPa to compute density from V_p as follows (Birch, 1961; Iturrino et al., 1991):

$$\rho = 0.335 + 0.5689 \times V_p.$$

CONCLUSIONS

1. The compressional and shear velocities at 200 MPa for ODP Leg 176 are within the experimental error of values obtained during Leg 118.
2. The Leg 176 measurements corroborate the Leg 118 observations that oceanic gabbros have low *Q* values (high attenuations).

F5. Shear wave attenuation computation, p. 17.

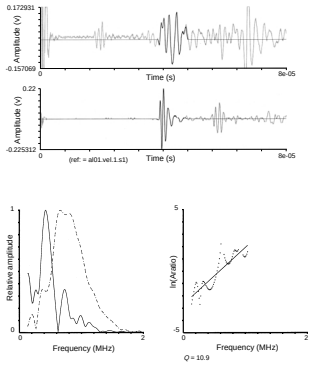

T2. Compressional and shear wave velocities, p. 19.

ACKNOWLEDGMENTS

This research used samples and/or data provided by the Ocean Drilling Program (ODP). ODP is sponsored by the U.S. National Science Foundation (NSF) and participating countries under management of Joint Oceanographic Institutions (JOI), Inc. Funding for this research was provided by a grant from the United States Science Support Program, Award #F000774 and the National Science Foundation Grant No. OCE-9730588.

REFERENCES

Birch, F., 1961. The velocity of compressional waves in rocks to 10 kilobars, 2. *J. Geophys. Res.,* 66:2199–2224.

Coyner, K.B., 1984. Effects of stress, pore pressure, and pore fluids on bulk strain, velocity, and permeability in rocks [Ph.D. dissert.]. MIT, Cambridge, MA.

Goldberg, D., Badri, M., and Wefer, W., 1991. Ultrasonic attenuation measurements in gabbros from Hole 735B. *In* Von Herzen, R.P., Robinson, P.T., et al., *Proc. ODP, Sci. Results,* 118: College Station, TX (Ocean Drilling Program), 253–260.

————, 1992. Acoustic attenuation in oceanic gabbro. *Geophys. J. Int.,* 111:193–202.

Iturrino, G.J., Christensen, N.I., Kirby, S., and Salisbury, M.H., 1991. Seismic velocities and elastic properties of oceanic gabbroic rocks from Hole 735B. *In* Von Herzen, R.P., Robinson, P.T., et al., *Proc. ODP, Sci. Results,* 118: College Station, TX (Ocean Drilling Program), 227–244.

Ludwig, W.J., Nafe, J.E., Drake, C.L., 1970. Seismic refraction. *In* Maxwell, A.E., *The Sea* (Vol. 4, Part 1): New York (John Wiley and Sons), 53–84.

Shipboard Scientific Party, 1989. Site 735. *In* Robinson, P.T., Von Herzen, R., et al., *Proc. ODP, Init. Repts.,* 118: College Station, TX (Ocean Drilling Program), 89–222.

————, 1999. Site 735. *In* Dick, H.J.B., Natland, J.H., Miller, D.J., et al., *Proc. ODP, Init. Repts.,* 176, 1–314 [CD-ROM]. Available from: Ocean Drilling Program, Texas A&M University, College Station, TX 77845-9547, U.S.A.

Swift, S.A., Hoskins, H., and Stephen, R.A., 1991. Seismic stratigraphy in a transverse ridge, Atlantis II Fracture Zone. *In* Von Herzen, R.P., Robinson, P.T., et al., *Proc. ODP, Sci. Results,* 118: College Station, TX (Ocean Drilling Program), 219–226.

Swift, S.A., and Stephen, R.A., 1992. How much gabbro is in ocean seismic Layer 3? *Geophys. Res. Lett.,* 19:1871–1874.

Toksöz, M.N., Johnston, D.H., and Timur, A., 1979. Attenuation of seismic waves in dry and saturated rock: I. Laboratory measurements. *Geophysics,* 44:681–690.

Von Herzen, R.P., Dick, H.J.B., and Robinson, P., 1991. Downhole measurements and physical properties, Hole 735B: summary and tectonic relationships. *In* Von Herzen, R.P., Robinson, P.T., et al., *Proc. ODP, Sci. Results,* 118: College Station, TX (Ocean Drilling Program), 553–557.

APPENDIX A

Compressional Velocity, Shear Velocity, Density, and Porosity as Functions of Pressure to 200 MPa

Core, section, interval (cm)	P_c (MPa)	P_p (MPa)	V_p (m/s)	$V_{s\text{-}1}$ (m/s)	$V_{s\text{-}2}$ (m/s)	Bulk density (g/cm^3) Saturated	Bulk density (g/cm^3) Dry	Saturation porosity (%)
176-735B-								
117R-1, 36–38								
0	9.9	2.1	6615	3699	3734	2.995	2.989	0.63
1	20.1	2.1	6662	3714	3749	2.995	2.989	0.63
2	40.1	2.1	6709	3729	3764	2.995	2.989	0.63
3	60.0	2.1	6662	3758	3779	2.995	2.989	0.63
4	60.2	2.1	6569	3758	3764	2.995	2.989	0.63
5	60.1	2.1	6709	3789	3749	2.995	2.989	0.63
6	80.1	2.1	6709	3758	3779	2.995	2.989	0.63
7	100.2	2.1	6662	3743	3764	2.995	2.989	0.63
8	150.0	2.2	6661	3758	3764	2.995	2.989	0.63
9	150.1	2.1	6662	3758	3779	2.995	2.989	0.63
10	150.1	2.1	6615	3758	3795	2.995	2.989	0.63
11	200.0	2.1	6662	3758	3795	2.995	2.989	0.63
12	100.1	2.2	6615	3758	3795	2.995	2.989	0.63
13	60.1	2.1	6709	3758	3764	2.995	2.989	0.63
14	60.2	2.1	6662	3773	3764	2.995	2.989	0.63
15	60.3	2.0	6757	3714	3764	2.995	2.989	0.63
16	10.1	2.1	6615	3729	3734	2.995	2.989	0.63
146R-2, 0–7								
0	10.0	2.0	6547	3263	3265	2.877	2.873	0.40
1	20.4	1.9	6656	3320	3298	2.877	2.873	0.40
2	40.1	2.0	6706	3375	3332	2.877	2.873	0.40
3	60.2	2.0	6754	3401	3357	2.877	2.873	0.40
4	59.9	2.1	6733	3386	3367	2.877	2.873	0.40
5	60.2	2.0	6749	3406	3374	2.877	2.873	0.40
6	80.2	2.0	6719	3427	3403	2.877	2.873	0.40
7	100.4	1.9	6721	3464	3434	2.877	2.873	0.40
8	150.1	1.9	6768	3498	3487	2.877	2.873	0.40
9	150.1	2.0	6800	3496	3493	2.877	2.873	0.40
10	150.2	2.0	6781	3507	3482	2.877	2.873	0.40
11	200.1	2.0	6822	3513	3515	2.877	2.873	0.40
12	100.3	2.0	6811	3475	3461	2.877	2.873	0.40
13	60.4	2.0	6786	3437	3403	2.877	2.873	0.40
14	60.1	2.1	6751	3437	3413	2.877	2.873	0.40
15	60.0	2.1	6754	3416	3408	2.877	2.873	0.40
16	10.1	2.0	6548	3263	3269	2.877	2.873	0.40
146R-2, 8–11								
0	10.0	2.1	6404	3393	3404	2.808	2.804	0.42
1	20.3	2.0	6540	3454	3467	2.808	2.804	0.42
2	40.0	2.2	6681	3536	3542	2.808	2.804	0.42
3	60.1	2.1	6750	3576	3571	2.808	2.804	0.42
4	60.2	2.1	6759	3582	3581	2.808	2.804	0.42
5	60.1	2.1	6758	3594	3582	2.808	2.804	0.42
6	80.2	2.1	6784	3601	3594	2.808	2.804	0.42
7	100.0	2.2	6842	3625	3619	2.808	2.804	0.42
8	150.0	2.1	6922	3654	3669	2.808	2.804	0.42
9	150.1	2.1	6932	3669	3672	2.808	2.804	0.42
10	150.1	2.2	6922	3673	3681	2.808	2.804	0.42
11	199.8	2.2	6996	3703	3717	2.808	2.804	0.42
12	100.1	2.2	6862	3643	3633	2.808	2.804	0.42
13	60.1	2.2	6759	3609	3600	2.808	2.804	0.42
14	60.2	2.1	6759	3601	3596	2.808	2.804	0.42
15	60.0	2.2	6769	3598	3588	2.808	2.804	0.42
16	10.0	2.1	6549	3500	3483	2.808	2.804	0.42
146R-2, 11–14								
0	9.9	2.1	7269	3396	3579	3.077	3.071	0.55
1	20.0	2.1	7352	3494	3746	3.077	3.071	0.55
2	40.1	2.1	7437	3627	3787	3.077	3.071	0.55
3	60.1	2.1	7466	3875	3848	3.077	3.071	0.55
4	60.0	2.2	7495	3844	3863	3.077	3.071	0.55
5	60.2	2.1	7524	3837	3879	3.077	3.071	0.55

Appendix A (continued).

Core, section, interval (cm)	P_c (MPa)	P_p (MPa)	V_p (m/s)	$V_{s\text{-}1}$ (m/s)	$V_{s\text{-}2}$ (m/s)	Bulk density (g/cm³)		Saturation porosity (%)
						Saturated	Dry	
6	80.1	2.1	7524	3822	3886	3.077	3.071	0.55
7	100.2	2.1	7524	3799	3910	3.077	3.071	0.55
8	150.0	2.2	7554	3784	3934	3.077	3.071	0.55
9	150.0	2.2	7554	3791	3934	3.077	3.071	0.55
10	150.2	2.1	7626	3777	3926	3.077	3.071	0.55
11	200.2	2.0	7554	3802	3942	3.077	3.071	0.55
12	100.1	2.2	7554	3822	3934	3.077	3.071	0.55
13	60.0	2.2	7524	3860	3902	3.077	3.071	0.55
14	60.4	2.1	7554	3829	3918	3.077	3.071	0.55
15	60.0	2.2	7584	3829	3926	3.077	3.071	0.55
16	9.9	2.2	6879	3711	3596	3.077	3.071	0.55
165R-5, 70–72								
0	9.8	2.2	6476	3539	3529	2.962	2.958	0.41
1	20.4	2.0	6561	3597	3567	2.962	2.958	0.41
2	40.1	2.1	6717	3656	3606	2.962	2.958	0.41
3	60.0	2.2	6809	3697	3659	2.962	2.958	0.41
4	60.4	2.0	6833	3691	3673	2.962	2.958	0.41
5	59.9	2.2	6772	3718	3686	2.962	2.958	0.41
6	80.3	2.1	6856	3732	3693	2.962	2.958	0.41
7	100.3	2.1	6856	3746	3693	2.962	2.958	0.41
8	150.3	2.1	6928	3775	3735	2.962	2.958	0.41
9	150.1	2.1	6833	3760	3735	2.962	2.958	0.41
10	150.3	2.1	6833	3775	3745	2.962	2.958	0.41
11	200.1	2.1	6928	3811	3749	2.962	2.958	0.41
12	100.1	2.2	6928	3768	3721	2.962	2.958	0.41
13	60.1	2.2	6904	3739	3707	2.962	2.958	0.41
14	60.2	2.1	6904	3739	3707	2.962	2.958	0.41
15	60.1	2.1	6880	3753	3707	2.962	2.958	0.41
16	10.1	2.1	6476	3616	3561	2.962	2.958	0.41
165R-5, 73–76								
0	10.0	2.1	6769	3658	3647	2.958	2.953	0.51
1	20.1	2.1	6817	3694	3668	2.958	2.953	0.51
2	39.9	2.1	6916	3737	3704	2.958	2.953	0.51
3	60.1	2.1	6891	3760	3748	2.958	2.953	0.51
4	60.3	2.0	6916	3789	3785	2.958	2.953	0.51
5	60.2	2.1	6941	3805	3792	2.958	2.953	0.51
6	80.1	2.1	6967	3820	3808	2.958	2.953	0.51
7	100.0	2.1	6967	3828	3815	2.958	2.953	0.51
8	150.4	1.9	6992	3859	3870	2.958	2.953	0.51
9	150.1	2.1	6941	3859	3862	2.958	2.953	0.51
10	150.3	2.0	7044	3866	3870	2.958	2.953	0.51
11	200.1	2.1	7018	3882	3893	2.958	2.953	0.51
12	100.2	2.1	6992	3859	3854	2.958	2.953	0.51
13	60.2	2.1	7018	3851	3846	2.958	2.953	0.51
14	60.4	2.0	6992	3851	3838	2.958	2.953	0.51
15	60.3	2.0	7018	3851	3854	2.958	2.953	0.51
16	10.0	2.1	6362	3610	3592	2.958	2.953	0.51
165R-5, 76–82								
0	9.9	2.1	6716	3548	3545	2.966	2.961	0.52
1	20.0	2.1	6716	3572	3562	2.966	2.961	0.52
2	40.1	2.0	6716	3607	3627	2.966	2.961	0.52
3	60.1	2.0	6772	3649	3646	2.966	2.961	0.52
4	60.2	2.0	6857	3668	3670	2.966	2.961	0.52
5	60.0	2.1	6857	3680	3664	2.966	2.961	0.52
6	80.1	2.1	6857	3693	3701	2.966	2.961	0.52
7	100.0	2.1	6857	3705	3695	2.966	2.961	0.52
8	150.1	2.1	6886	3750	3727	2.966	2.961	0.52
9	150.1	2.1	6857	3737	3714	2.966	2.961	0.52
10	150.2	2.0	6886	3763	3740	2.966	2.961	0.52
11	200.0	2.1	7004	3776	3772	2.966	2.961	0.52
12	100.1	2.1	6857	3724	3720	2.966	2.961	0.52
13	60.2	2.0	6886	3724	3701	2.966	2.961	0.52
14	60.3	1.9	6886	3718	3701	2.966	2.961	0.52
15	59.9	2.1	6857	3724	3695	2.966	2.961	0.52
16	9.9	2.1	6661	3589	3562	2.966	2.961	0.52

Appendix A (continued).

Core, section, interval (cm)	P_c (MPa)	P_p (MPa)	V_p (m/s)	$V_{s\text{-}1}$ (m/s)	$V_{s\text{-}2}$ (m/s)	Bulk density (g/cm³)		Saturation porosity (%)
						Saturated	Dry	
193R-1, 94–96								
0	9.9	2.1	6407	3334	3270	2.945	2.940	0.49
1	20.0	2.1	6578	3427	3377	2.945	2.940	0.49
2	40.0	2.1	6622	3488	3424	2.945	2.940	0.49
3	60.0	2.1	6690	3519	3472	2.945	2.940	0.49
4	60.0	2.2	6690	3544	3484	2.945	2.940	0.49
5	59.9	2.2	6712	3551	3490	2.945	2.940	0.49
6	80.1	2.1	6735	3577	3522	2.945	2.940	0.49
7	100.1	2.1	6758	3596	3534	2.945	2.940	0.49
8	150.4	2.0	6758	3649	3579	2.945	2.940	0.49
9	150.2	2.1	6805	3656	3579	2.945	2.940	0.49
10	150.0	2.1	6782	3649	3592	2.945	2.940	0.49
11	199.9	2.2	6852	3697	3625	2.945	2.940	0.49
12	100.0	2.2	6712	3616	3553	2.945	2.940	0.49
13	60.2	2.1	6690	3570	3515	2.945	2.940	0.49
14	59.9	2.2	6712	3577	3509	2.945	2.940	0.49
15	60.1	2.1	6712	3570	3522	2.945	2.940	0.49
16	10.1	2.1	6556	3439	3331	2.945	2.940	0.49
193R-1, 97–99								
0	10.0	2.1	6366	3311	3257	2.924	2.919	0.55
1	20.0	2.1	6564	3388	3366	2.924	2.919	0.55
2	40.0	2.1	6609	3425	3391	2.924	2.919	0.55
3	60.2	2.1	6609	3431	3397	2.924	2.919	0.55
4	59.9	2.1	6587	3437	3397	2.924	2.919	0.55
5	60.0	2.1	6656	3443	3415	2.924	2.919	0.55
6	80.2	2.1	6703	3475	3415	2.924	2.919	0.55
7	100.4	2.0	6703	3488	3440	2.924	2.919	0.55
8	150.1	2.1	6726	3546	3490	2.924	2.919	0.55
9	150.1	2.1	6774	3546	3484	2.924	2.919	0.55
10	150.1	2.1	6703	3553	3497	2.924	2.919	0.55
11	199.9	2.1	6823	3593	3562	2.924	2.919	0.55
12	100.3	2.1	6679	3513	3471	2.924	2.919	0.55
13	60.3	2.1	6703	3456	3440	2.924	2.919	0.55
14	60.2	2.1	6679	3475	3452	2.924	2.919	0.55
15	60.1	2.1	6679	3469	3452	2.924	2.919	0.55
16	10.2	2.1	6430	3300	3240	2.924	2.919	0.55
193R-1, 100–106								
0	10.1	2.1	6316	3195	3240	2.905	2.898	0.67
1	20.1	2.1	6441	3321	3329	2.905	2.898	0.67
2	40.0	2.1	6595	3457	3447	2.905	2.898	0.67
3	60.1	2.1	6640	3513	3503	2.905	2.898	0.67
4	60.2	2.1	6663	3526	3507	2.905	2.898	0.67
5	60.2	2.1	6685	3539	3500	2.905	2.898	0.67
6	80.1	2.2	6732	3565	3513	2.905	2.898	0.67
7	100.2	2.1	6779	3591	3532	2.905	2.898	0.67
8	150.1	2.1	6803	3631	3578	2.905	2.898	0.67
9	150.1	2.1	6851	3631	3584	2.905	2.898	0.67
10	150.2	2.1	6851	3645	3584	2.905	2.898	0.67
11	200.2	2.1	6899	3673	3611	2.905	2.898	0.67
12	100.4	2.0	6779	3604	3552	2.905	2.898	0.67
13	60.4	2.1	6732	3571	3526	2.905	2.898	0.67
14	60.2	2.1	6732	3578	3526	2.905	2.898	0.67
15	60.1	2.2	6709	3558	3526	2.905	2.898	0.67
16	10.1	2.1	6399	3309	3276	2.905	2.898	0.67
196R-4, 93–95								
0	10.0	2.1	6325	3284	3151	2.823	2.818	0.49
1	20.0	2.1	6461	3447	3301	2.823	2.818	0.49
2	40.0	2.1	6602	3671	3520	2.823	2.818	0.49
3	59.9	2.1	6801	3876	3648	2.823	2.818	0.49
4	60.2	2.1	6853	3893	3648	2.823	2.818	0.49
5	60.1	2.1	6750	3876	3648	2.823	2.818	0.49
6	80.2	2.1	6801	3927	3707	2.823	2.818	0.49
7	100.2	2.1	6801	3961	3760	2.823	2.818	0.49
8	150.1	2.1	6801	3996	3817	2.823	2.818	0.49
9	150.2	2.0	6905	4021	3833	2.823	2.818	0.49
10	150.1	2.1	6853	4014	3833	2.823	2.818	0.49
11	199.9	2.1	7013	4050	3856	2.823	2.818	0.49

Appendix A (continued).

Core, section, interval (cm)	P_c (MPa)	P_p (MPa)	V_p (m/s)	$V_{s\text{-}1}$ (m/s)	$V_{s\text{-}2}$ (m/s)	Bulk density (g/cm³)		Saturation porosity (%)
						Saturated	Dry	
12	100.0	2.2	6905	3927	3817	2.823	2.818	0.49
13	60.0	2.2	6959	3910	3723	2.823	2.818	0.49
14	60.2	2.1	6959	3910	3692	2.823	2.818	0.49
15	60.0	2.1	6959	3910	3677	2.823	2.818	0.49
16	10.0	2.1	6507	3421	3265	2.823	2.818	0.49
208R-5, 106–108								
0	9.8	2.2	7212	3902	4066	3.214	3.208	0.60
1	20.0	2.1	7270	3953	4121	3.214	3.208	0.60
2	39.9	2.1	7448	4058	4197	3.214	3.208	0.60
3	59.9	2.1	7328	4095	4197	3.214	3.208	0.60
4	60.1	2.1	7387	4095	4216	3.214	3.208	0.60
5	60.1	2.1	7448	4095	4216	3.214	3.208	0.60
6	79.9	2.1	7509	4076	4216	3.214	3.208	0.60
7	99.9	2.2	7448	4095	4197	3.214	3.208	0.60
8	149.8	2.1	7448	4113	4216	3.214	3.208	0.60
9	150.0	2.1	7448	4132	4216	3.214	3.208	0.60
10	150.0	2.1	7448	4151	4255	3.214	3.208	0.60
11	199.9	2.1	7509	4151	4275	3.214	3.208	0.60
12	100.0	2.2	7448	4151	4236	3.214	3.208	0.60
13	60.2	2.0	7571	4132	4236	3.214	3.208	0.60
14	60.2	2.1	7509	4132	4236	3.214	3.208	0.60
15	60.0	2.2	7509	4132	4236	3.214	3.208	0.60
16	10.0	2.1	7328	3919	4185	3.214	3.208	0.60

Note: P_p = pore pressure, P_c = confining pressure, V_p = compressional wave velocity, V_s = shear wave velocity.

APPENDIX B

Compressional and Shear Wave Attenuation as Functions of Pressure to 200 MPa

Core, section, interval (cm)	Depth (mbsf)	Q_p 60 MPa	Q_p 100 MPa	Q_p 150 MPa	Q_p 200 MPa	Q_p 60 MPa	Q_{s-1} 60 MPa	Q_{s-1} 100 MPa	Q_{s-1} 150 MPa	Q_{s-1} 200 MPa	Q_{s-1} 60 MPa	Q_{s-2} 60 MPa	Q_{s-2} 100 MPa	Q_{s-2} 150 MPa	Q_{s-2} 200 MPa	Q_{s-2} 60 MPa
176-735B-																
117R-1, 36–38	117.36	13.6	15.6	21.9	23.4	14.2	9.59	13	13.2	13.5	10.5	8.08	12.9	23.5	27.7	9.04
146R-2, 0–7	146.0	14.2	15.7	17.7	18	15	5.98	10.4	10.9	11	8.49	8.57	11.1	14.5	17.9	8.54
146R-2, 11–14	146.11	20.7	22.7	25.2	28.1	21.5	10.4	15.3	18.8	22	10.4	12.2	17.2	21.3	22.6	13.1
146R-2, 8–11	146.8	14.4	14.5	15.7	15.5	14.3	10.8	12.1	11.7	11.1	11	11.2	11.6	13.2	13.9	12.1
165R-5, 70–72	165.70	41.4	63.7	293	258	54.6	19.5	25	26.2	29.2	20.4	15.3	17.7	20.8	23.9	15.5
165R-5, 73–76	165.73	51	61.6	229	inf	54	24.5	30.3	29.5	31	25.8	13.2	16.9	19.8	20.5	13.7
165R-5, 76–82	165.76	38.1	44.8	61.9	92	35	12.8	14.3	15.4	17.4	13.1	11.5	13.4	15.4	16.8	11.7
193R-1, 100–106	193.100	16.7	24.9	34.3	36	17	16.1	19.1	19.9	20.2	16.7	13.2	16.3	18.2	18.6	13.5
193R-1, 94–96	193.94	23.3	31.6	45.3	46.2	23.6	13.6	17	17.4	16.6	13.8	13.7	18.1	20.7	21.3	14.3
193R-1, 97–99	193.97	16.4	21.2	27.8	28.1	16.7	11	14	16	15.9	11.7	11.2	14.9	17.9	19.5	13.1
208R-5, 106–108	208.106	11.8	13.3	18	18.2	11.9	8.2	10.6	10.2	10.2	8.32	6.2	7.87	9.46	10.9	6.25
196R-4, 93–95	196.93	11.3	14.9	20.1	19.5	11.3	5.76	6.78	7.7	5.62	6.09	6.17	7.6	9.79	11.5	6.33

Notes: Measurements were made by New England Research, Inc. Q = quality factor. Attenuation = 1000/Q. inf = there is no measurable attenuation.

Figure F1. Compressional wave velocity at 200 MPa is displayed as a function of porosity for selected cores from Hole 735B acquired during ODP Leg 176. In these very low porosity samples, with all values <0.75%, there does not appear to be a relationship between compressional wave velocity and porosity. It is generally assumed that at 200 MPa, pressures typical of the lower crust, all of the microcracks have been squeezed shut. Igneous lithology (Shipboard Scientific Party, 1999): o = olivine gabbro, + = gabbronorite, × = troctolitic gabbro.

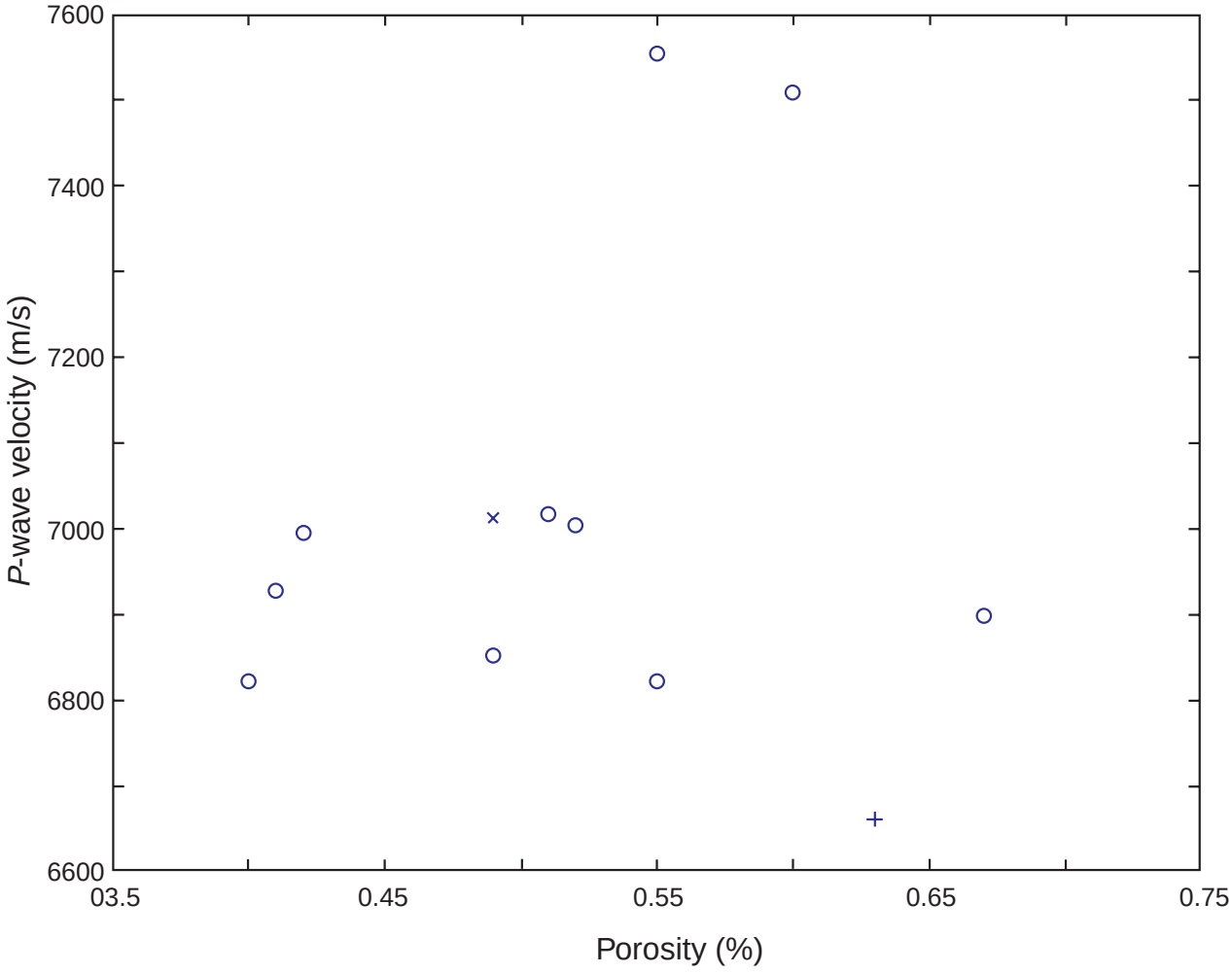

Figure F2. Compressional wave velocity at 200 MPa is displayed as a function of saturated bulk density for selected cores from Hole 735B acquired during ODP Leg 176. Also shown are the lines of constant mean atomic weight (M), based on Birch's Law (Birch, 1961; Iturrino et al., 1991). As for the Hole 735B samples acquired during Leg 118, the olivine gabbros cluster near the line M = 21. Igneous lithology (Shipboard Scientific Party, 1999): o = olivine gabbro, + = gabbronorite, × = troctolitic gabbro.

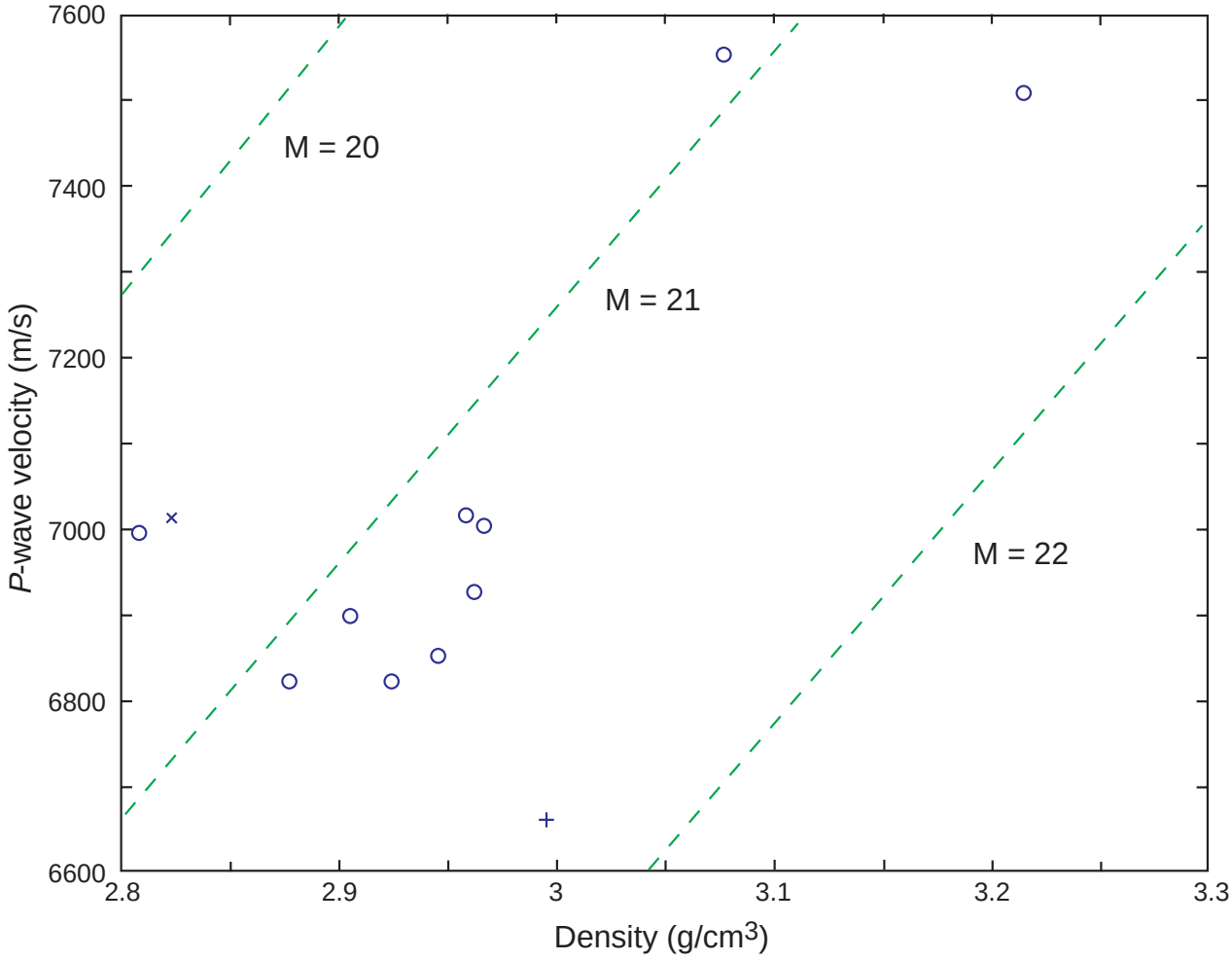

Figure F3. Compressional wave velocity at 200 MPa is displayed as a function of shear wave velocity for selected cores from Hole 735B acquired during ODP Leg 176. Also shown are the lines of constant Poisson's ratio (σ). The average Poisson's ratio in these samples is higher than the average for the Hole 735B samples acquired during Leg 118. None of the Leg 118 samples had Poisson's ratios >0.30. Igneous lithology (Shipboard Scientific Party, 1999): o = olivine gabbro, + = gabbronorite, × = troctolitic gabbro.

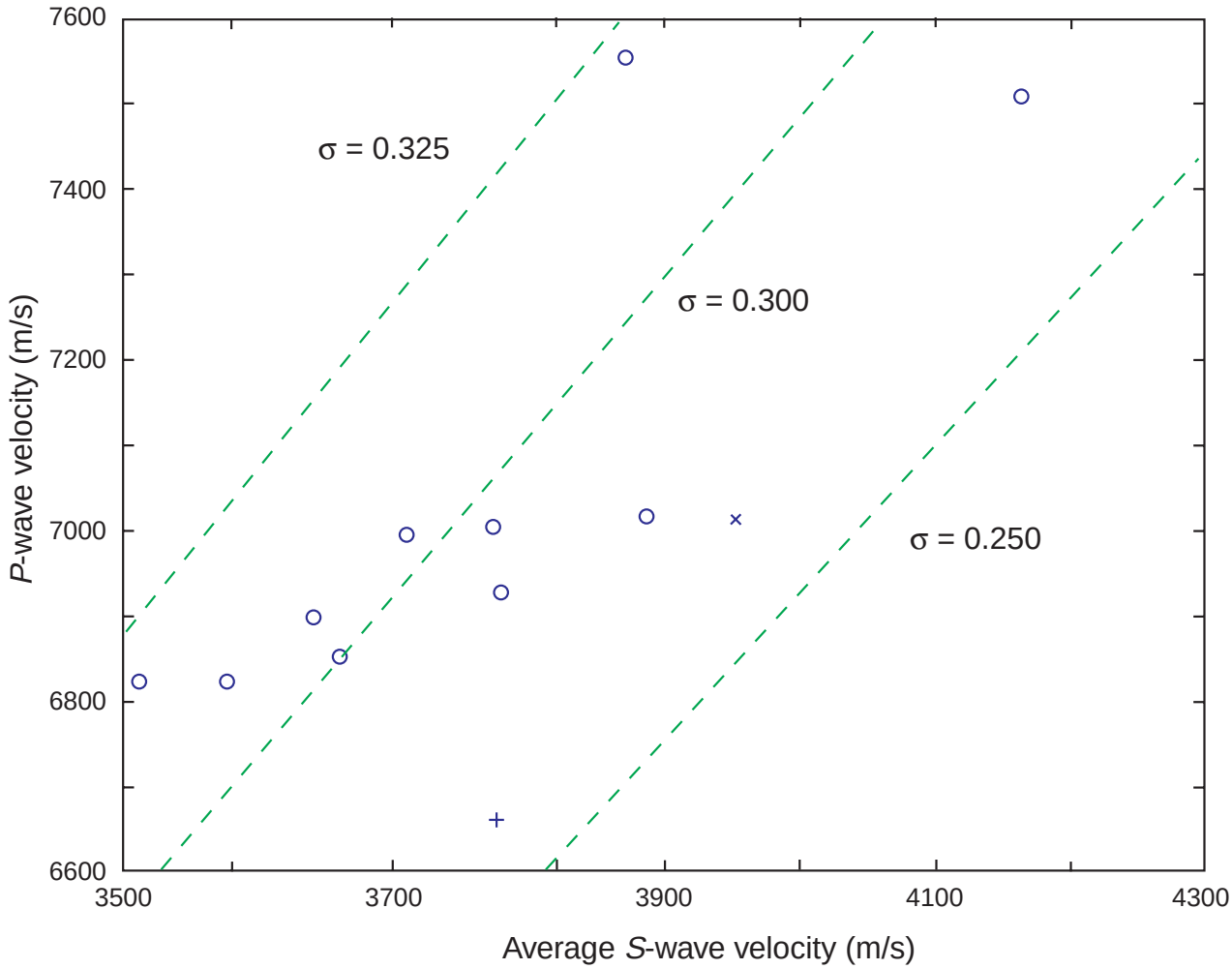

Figure F4. The spectral ratio method is applied to obtain compressional wave attenuation by comparing the spectra from an aluminum reference to the spectra for a gabbro sample. **A.** Time series of the pulse through gabbro. The spectra is computed for the waveform with a bold line. **B.** The pulse through the aluminum reference is unattenuated. **C.** The spectra are compared: solid line = gabbro, dashed line = aluminum. The loss of high frequencies due to attenuation in the gabbro is evident. **D.** The natural logarithm of the ratio of the two spectra is displayed as a function of frequency as open circles. The solid line through these open circles is the least-squares fit line. For intrinsic attenuation in an infinite, homogeneous medium, theory predicts that the natural logarithm of spectral ratios should be a straight line. Q is computed from the slope (m) of the ratio of the spectral values of the aluminum to the gabbro as follows: $Q = \pi\, x_{gab}/(c \times m)$, where x_{gab} = the propagation distance in gabbro, and c = the compressional velocity in gabbro. In this case, $Q = 17.7$. (**Figure shown on next page.**)

Figure F4 (continued). (Caption shown on previous page.)

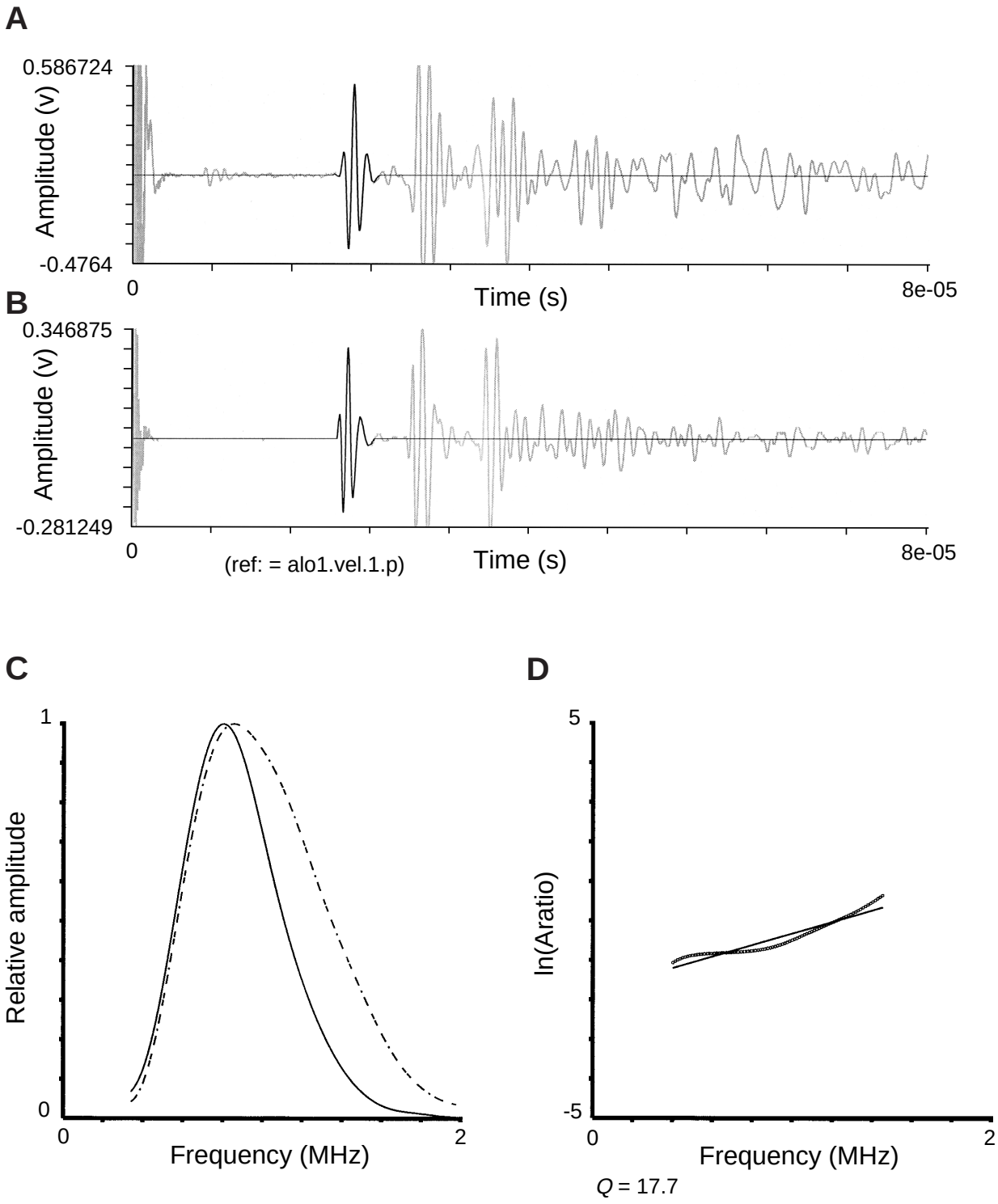

Figure F5. The shear wave attenuation is computed using the same procedure as outlined in Figure F4, p. 15, but substituting the shear velocity for *c*. In the shear case, however, the waveforms are much more distorted during propagation through the gabbro (top plot). The slope of the spectral ratios, which is used to compute *Q*, is highly nonlinear, and the shear attenuation value (*Q* = 10.9) is suspect.

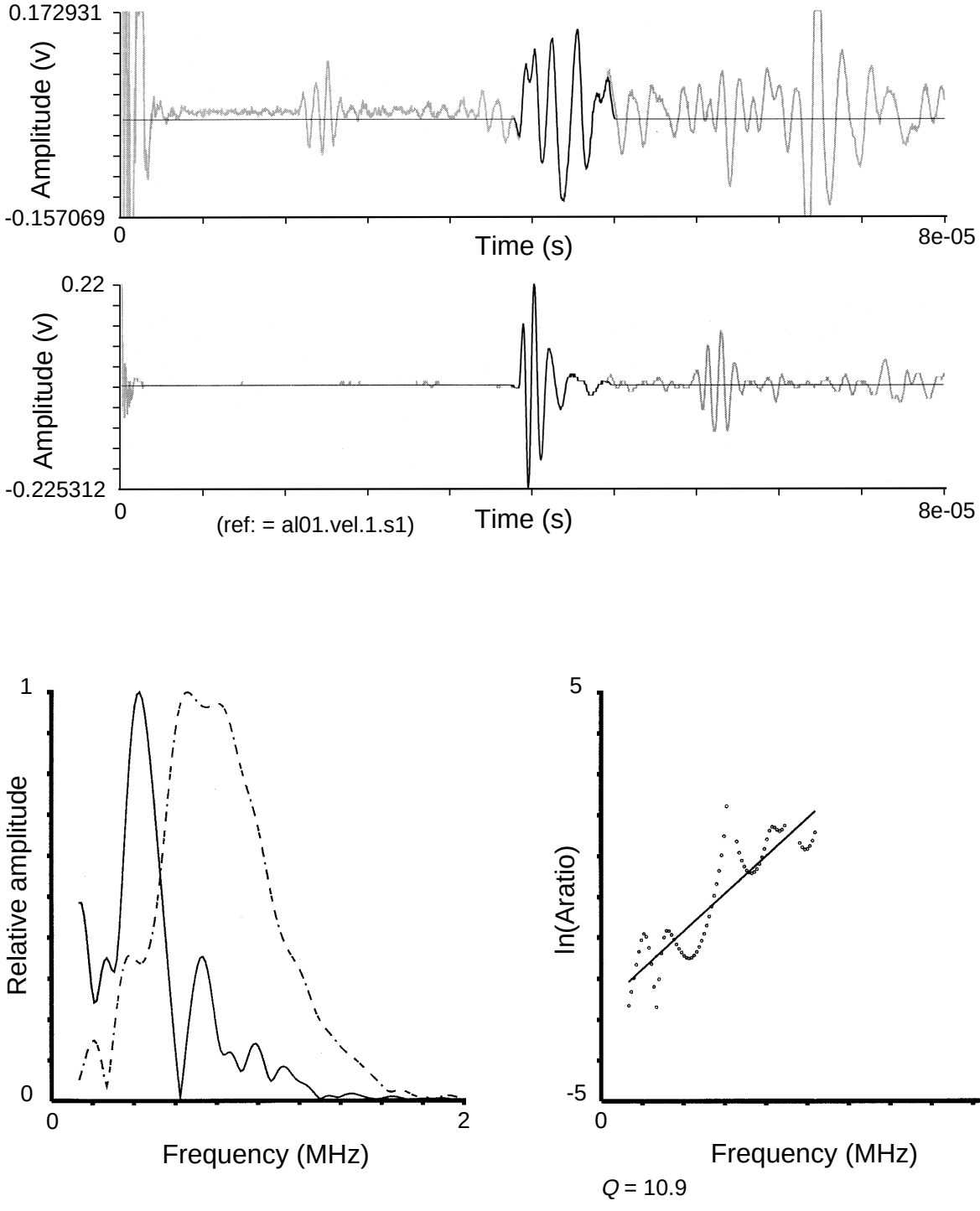

Table T1. Summary of cores selected for shore-based analysis.

Core, section, interval (cm)	Depth (mbsf)	Volume (cm^3)	Piece	Description
176-735B-				
117R-1, 36–38	681.56	10	3A	MC, gabbronorite
146R-2, 0–7	932.79	20	1A	Whole-core MC–Z
146R-2, 8–11	932.87	20	1A	Whole-core MC–X
146R-2, 11–14	932.9	20	1A	Whole-core MC–Y, olivine gabbro
165R-5, 70–72	1110.79	20	2	Whole-core MC–Y
165R-5, 73–76	1110.82	20	2	Whole-core MC–X
165R-5, 76–82	1110.85	25	2	Whole-core MC–Z, olivine gabbro
193R-1, 94–96	1355.94	20	3B	Whole-core MC–Y
193R-1, 97–99	1355.97	20	3B	Whole-core MC–X
193R-1, 100–106	1356	25	3B	Whole-core MC–Z, olivine gabbro
196R-4, 93–95	1378.09	10	7A	PMAG MC–high attenuation, troctolitic gabbro
208R-5, 106–108	1485.2	10	3C	PMAG MC–7.8 km/s, olivine gabbro

Note: MC = minicore, PMAG = paleomagnetism.

Table T2. Compressional and shear wave velocities of three-axis minicores at 200 MPa.

Core, section	146-2		165-5		193-1	
	Raw	Corrected	Raw	Corrected	Raw	Corrected
Compressional wave velocity, V_p (m/s):						
x	6996	7246	7018	7004	6823	6869
y	7554	7331	6928	6907	6852	6861
z	6822	6950	7004	6976	6899	6978
Shear wave velocity 1, V_s (m/s):						
x	3703	3838	3882	3874	3593	3618
y	3802	3681	3811	3800	3697	3702
z	3513	3582	3776	3761	3673	3716
Shear wave velocity 2, V_s (m/s):						
x	3717	3852	3893	3885	3562	3587
y	3942	3821	3749	3738	3625	3630
z	3515	3584	3772	3757	3611	3654

Note: The "raw" data have been "corrected" for density variations.